Materials Today Communications 32 (2022) 104059

Contents lists available at ScienceDirect

Materials Today Communications

journal homepage: www.elsevier.com/locate/mtcomm

Predicting mechanical properties of high entropy alloys with face centered cubic structure from first principles calculations

Siming Zhang, Guofeng Wang *

Department of Mechanical Engineering and Materials Science, University of Pittsburgh, PA 15261, USA

ARTICLE INFO

Keywords:
High entropy alloy
First principles calculation
Elastic constant
Stacking fault energy
Yield strength

ABSTRACT

High-entropy alloys (HEAs) are a class of solid-solution alloys with multiple equal or nearly-equal molar constituents and found to exhibit excellent mechanical properties. In this study, we have developed the first-principles density functional theory based computational methods to predict the elastic constants and yield strength of the HEAs with face centered cubic (fcc) crystal structure. Moreover, the developed computational methods were applied to four fcc HEAs including CoFeNi, CoCrFeNi, CoCrFeCuNi, and RhIrPdPtNiCu with equal molar composition. Specifically, we predicted the Young's modulus to be 204 GPa for CoFeNi, 226 GPa for CoCrFeNi, 217 GPa for CoCrFeCuNi, and 213 GPa for RhIrPdPtNiCu, and the yield strength to be 232 MPa for CoFeNi, 268 MPa for CoCrFeNi, 212 MPa for CoCrFeCuNi, and 520 MPa for RhIrPdPtNiCu. These computational predicted values are found to agree well with available experimental data. Therefore, these first-principles calculation methods can be used for expedite optimization on the mechanical properties of HEAs across vast composition space.

1. Introduction

High entropy alloy (HEA) refers to a class of multicomponent alloys, with five or more components, in equal or nearly equal concentrations, and forming simple solid solution phase [1–3]. Many HEAs have been found to exhibit impressive mechanical properties. For example, CrMnFeCoNi HEA (also known as Cantor alloy) has a remarkable combination of strength and ductility (yield strength of 300–350 MPa, ultimate tensile strength of 920 MPa and 52% elongation) [4,5]. Moreover, it was reported that CrMnFeCoNi HEA possesses high fracture toughness as ~220 MPa $m^{0.5}$ [6]. Consequently, the HEAs have potential applications as high-performance structural materials, with the mechanical properties rivaling those of stainless steel (yield strength of 220 MPa, ultimate tensile strength of 520–670 MPa, 45% elongation [7], and ~100 MPa $m^{0.5}$ fracture toughness [6]). In addition, the mechanical properties of HEAs can be tuned by varying their compositions. For instance, it has been reported that the yield strength of Fex $(CoCrMnNi)_{100-x}$ HEAs would reduce from 310 MPa to 160 MPa with an increase of x from 20 to 60 [8], whereas the yield strength of $Al_xCoCrNi$ HEAs would increase from 250 MPa to 310 MPa with an increase of the atomic percentage of Al content from 0% to 7% [9].

To enable rational design of HEAs for specific technical applications, accurate prediction of their mechanical properties as a function of their chemical composition is desired [2]. Two types of the DFT based computational approaches have already been developed to predict the elastic properties of HEAs. One computational approach is based on the single-site coherent-potential approximation (CPA) [10], which assumes that each lattice site is occupied by a pseudo atom representing the overall composition of the alloy. With this computational method, the Young's modulus of CrFeMnCoNi HEA was predicted to be 267 GPa, 32% higher than experimental value of 202 GPa [11,12], and the Young's modulus of CoCrFeNi HEA to be 242 GPa [13], 13% higher than experimental value of 215 GPa [14]. The other computational approach is based on the special quasi-random structures [15,16], which assumes that the solid solution structure of a HEA can be obtained by minimizing pair correlation functions on each site. Using this computational method, Kim et al. predicted the shear modulus of $Al_{0.3}$CoCrFeNi HEA to be 85 GPa, about 5% higher than experimental value of 81 GPa [17], and the Young's modulus of CoCrFeNi HEA could be derived to 195 GPa, about 9% lower than experimental value of 215 GPa [14].

In comparison, the DFT based computational approach to predict the yield strength of HEAs is scarce. A notable work is that Yin et al. proposed a computational approach based on solid solution strengthening theory and using the DFT computed values of misfit volumes as inputs

* Corresponding author.
E-mail address: guw8@pitt.edu (G. Wang).

https://doi.org/10.1016/j.mtcomm.2022.104059
Received 6 May 2022; Received in revised form 14 July 2022; Accepted 17 July 2022
Available online 19 July 2022

[18]. This computational approach has been successfully applied to predict the yield strength of RhIrPdPtNiCu HEA to be 583 MPa, in good agreement with experimental value of 527 MPa. However, the same DFT based computational approach led to significant underprediction of the yield strength of NiCoCr alloy [19].

In this study, we demonstrate a first-principles density functional theory (DFT) based computational approach to predict a series of mechanical properties (including elastic constants, Young's and shear modulus, stacking fault energies, twinnability parameter, Peierls stress and critical twinning stress, and yield strength) of HEAs with face-centered cubic (fcc) crystal structure. In particular, we proposed a new computational approach to predict the yield strength of fcc HEAs from the generalized stacking fault energy curve of the alloy. Moreover, we validated the proposed DFT based computational approach by examining its predictions for four different HEAs (i.e., CoFeNi, CoCrFeNi, CoCrFeCuNi, and RhIrPdPtNiCu) which have an fcc crystal structure and solid solution phase, but with dramatically different chemical compositions. We have found good agreement between the computational predictions and experimental values for both the elastic and plastic properties of these four fcc HEAs.

2. Computational method

In this study, all the spin-polarized DFT calculations were carried out using the Vienna ab initio simulation package (VASP) [20]. Plane wave basis associated with the projector augmented wave approach [21] was employed. The generalized gradient approximation (GGA) with the Perdew-Burke-Ernzerhof (PBE) [22] functional was used to evaluate the exchange-correlation energy. The plane wave energy cut-off energy was set to be 500 eV. In the calculations, the total energy of each system was converged within 10^{-6} eV. In elastic property calculations, we used a supercell containing 108 atoms for modelled CoFeNi, CoCrFeNi and RhIrPdPtNiCu HEAs, and a supercell containing 120 atoms for modelled CoCrFeCuNi HEA. A Monkhorst-Pack k-point [23] grids of $4 \times 4 \times 4$ and $4 \times 4 \times 3$ were used in these 108 and 120 atoms bulk crystal calculations, respectively. We used ten-layer or nine-layer slab cells to model (111) stacking faults. In the slab cells, a vacuum region of 12 Å thick was added in the direction normal to the (111) plane to minimize the influence of periodic images. The generalized stacking fault energy (GSFE) and generalized planar fault energy (GPFE) curves were predicted by calculating the energies of the slab cells in which the bottom half crystal was fixed while the top half crystal slipped along $[11\bar{2}]$ direction up to a full Burgers vector of a $a/6 < 11\bar{2} >$ Shockley partial dislocation. A Monkhorst-Pack k-point grid of $4 \times 4 \times 1$ was used for the (111) stacking fault calculations. All the structures were fully relaxed until the residual force acting on each atom was lower than 0.01 eV/Å.

3. Results and discussion

3.1. Elastic property predictions

In this work, we modelled the bulk crystal of CoFeNi and CoCrFeNi alloys using a cubic supercell containing 108 atoms and the bulk crystal of CoCrFeCuNi and RhIrPdPtNiCu alloys using an orthorhombic supercell containing 120 atoms. Moreover, we used ATAT code [24] to generate the special quasi-random structures of these four alloys to mimic the actual HEAs with equal molar composition. For example, the simulation model of the four-element CoCrFeNi HEA is illustrated in Fig. 1(a), showing homogenous mixing of the four constituent elements.

Moreover, we performed the DFT calculations to determine the equilibrium lattice constant for this structure by finding the minimum energy state as shown in Fig. 1(b). Our predictions of the lattice constants of these four HEAs are found to be very close the published values in the literature. Specifically, we predicted the lattice constant to be 3.56 Å (as compared to previous calculation value of 3.56 Å [25] and experimental value of 3.60 Å [26]) for CoFeNi alloy, 3.53 Å (as compared to previous calculation values ranging from 3.50 Å to 3.59 Å [25,27,28] and experimental value of 3.55 Å [29]) for CoCrFeNi, 3.56 Å (as compared to previous experimental value of 3.58 Å [30]) for CoCrFeCuNi, and 3.82 Å (as compared to previous calculation value of 3.81 Å [18]) for RhIrPdPtNiCu, respectively.

Using the optimized structure models of the four HEA single crystal, we predicted their elastic constants C_{11}, C_{12}, and C_{44} by applying the equal-axis volume expansion strain and volume conserving shear strains following the computational procedure proposed by Söderlind et al. [31] for cubic metals. Our predictions given in Table 1 are found to agree well with the computational values obtained from other DFT calculations. [13,18,32,33].

Furthermore, we evaluated the Young's modulus and shear modulus of the four HEAs in polycrystalline material form and also presented our predictions in Table 1. The Young's modulus was calculated using the formula $E = \frac{9BG_v}{3B+G_v}$, where G_v is the isotropic Voigt shear modulus (iso-strain assumption) $G_v = \frac{1}{5}(3C_{44} + C')$, [34] and B is the bulk modulus of the crystal. The shear modulus was calculated using the formula $G = \frac{1}{2}(G_v + G_R)$, where G_R is the isotropic Reuss shear modulus (iso-stress assumption) $G_R = \frac{5(C_{11}-C_{12})C_{44}}{(4C_{44}+3(C_{11}-C_{12}))}$.

G. Laplanche et al. measured the elastic moduli of the recrystallized CoFeNi and CoCrFeNi alloy samples using both torsion and bending

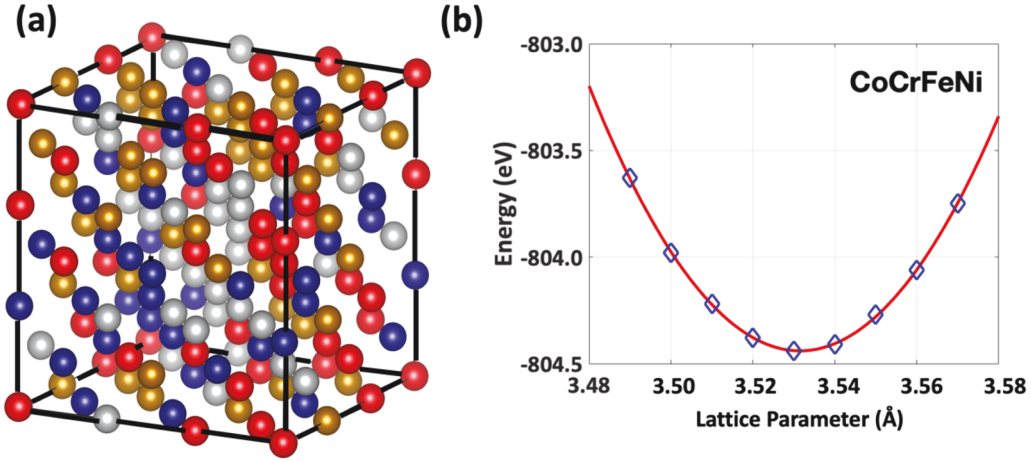

Fig. 1. (a) An atomistic structure of CoCrFeNi HEA in an fcc crystal structure. The blue, red, brown, and grey balls represent Co Cr, Fe, and Ni atoms, respectively. (b) Variation of the DFT calculated total energy with the lattice parameter of the simulation cell for the modelled CoCrFeNi HEA.

Table 1
Predicted elastic constants (C_{11}, C_{12}, and C_{44}) for single-crystal HEAs, and Young's modulus (E), shear modulus (G) for polycrystal HEAs using the DFT method.

		CoFeNi	CoCrFeNi	CoCrFeCuNi	RhIrPdPtNiCu
C_{11} (GPa)	This work	240	223	207	278
	Literature	222 [39]	219 [32]	209 [33]	289 [18]
C_{12} (GPa)	This work	152	124	145	162
	Literature	166 [39]	126 [32]	150 [33]	176 [18]
C_{44} (GPa)	This work	113	133	131	123
	Literature	110 [39]	130 [32]	142 [33]	112 [18]
E (GPa)	This work	204	226	217	213
G (GPa)	This work	78	85	71	84

mechanical tests in the temperature range of 293–1000 K. [35] Their measurement values at 293 K are E = 175 GPa, G = 68 GPa for CoFeNi and E = 214 GPa, G = 86 GPa for CoCrFeNi alloys. As compared to these experimental data, our DFT predicted elastic moduli given in Table 1 are within 16.6% difference for CoFeNi and within 5.6% difference for CoCrFeNi. No experimental elastic moduli values of CoCrFeCuNi, and RhIrPdPtNiCu alloys are available for comparison yet. Nevertheless, we can estimate their values using the rule of mixtures (ROM). Within ROM, the elastic modulus of HEAs could be calculated as $E = \sum x_i E_i$, where E_i is experimental value of elastic modulus of constituent element i (found from literatures [36–38]) and x_i is the molar ratio of constituent element i. The values estimated from ROM are E = 206 GPa, G = 80 GPa for CoCrFeCuNi and E = 237 GPa, G = 91 GPa for RhIrPdPtNiCu alloys. As compared to these data from ROM, our DFT predicted elastic moduli given in Table 1 are within 11.3% difference for CoCrFeCuNi and within 10.1% difference for RhIrPdPtNiCu.

3.2. Stacking fault energy predictions

Relevant to the plastic deformation of HEAs, we have further used the DFT computational method to predict the generalized stacking fault energy (GSFE) and generalized planar fault energy (GPFE) curves for CoFeNi, CoCrFeNi, CoCrFeCuNi, and RhIrPdPtNiCu HEAs. The staking faults in these fcc alloys were modelled using a simulation cell consisting of (111) atomic layers and a vacuum region separating the periodic images. We used a ten-layer (111) slab containing 160 atoms for CoCrFeNi and CoCrFeCuNi alloys, whereas a nine-layer (111) slab containing 144 atoms for CoFeNi and RhIrPdPtNiCu alloys. In each slab model, we constructed the special quasi-random structures of the alloys with equal molar composition.

In Fig. 2, we employ CoCrFeNi alloy as an example to illustrate the structures of various stacking faults. In a perfect fcc crystal (Fig. 2(a)), the (111) atomic layers are packed following a repeating sequence of "ABC" from the bottom to the top of the slab model along the [111] direction. We constructed an unstable stacking fault (USF) (Fig. 2(b)) and an intrinsic stacking fault (ISF) (Fig. 2(c)) by slipping the top five (111) atomic layers relative to the bottom ones along the $[11\bar{2}]$ direction by one half and a whole Burgers vector of $a/6 < 11\bar{2} >$ Shockley partial, where a is the lattice constant of the alloy, respectively. As compared to the perfect fcc crystal, one (111) atomic layer (labeled as "C" layer in Fig. 2) is missing in ISF which is a one-layer stacking fault. From this ISF structure, we further constructed an unstable twinning (UT) (Fig. 2(d)) and an extrinsic stacking fault (ESF) (Fig. 2(e)) by slipping the top four (111) atomic layers relative to the bottom ones along the $[11\bar{2}]$ direction by one half and a whole Burgers vector of $a/6 < 11\bar{2} >$ Shockley partial, respectively. It notes that ESF, as shown in Fig. 2(e), is a two-layer stacking fault. The formation energies of USF, ISF, UT, and ESF are defined as the area normalized energy difference between the corresponding stacking fault structures (Fig. 2(b-e)) and the reference fcc crystal (Fig. 2(a)).

In Fig. 3, we plot the calculated energies of these stacking faults. It can be seen from the GSFE and GPFE curves that the intrinsic stacking fault and extrinsic stacking fault are stable planar defects in the crystal. By contrast, the unstable stacking fault is a transition state from a local stacking of fcc (111) atomic layers to a one-layer stacking fault, and the unstable twining represents a transition state from a one-layer stacking fault to a two-layer stacking fault in the process of formation of twin boundary.

It was reported by Ding et al. that local chemical order could appreciably affect the calculated values of the stacking fault energies in CoCrNi medium-entropy solid-solution alloy [40]. In this study, we compared the stacking fault energies calculated using three different interfaces with different chemical compositions and atomic arrangements. For all the four HEAs, our results show negligible change in the values of stacking fault energies with such a change of interfaces. Nevertheless, all the stacking fault energies reported here are the average values calculated from three different interfaces. In this study,

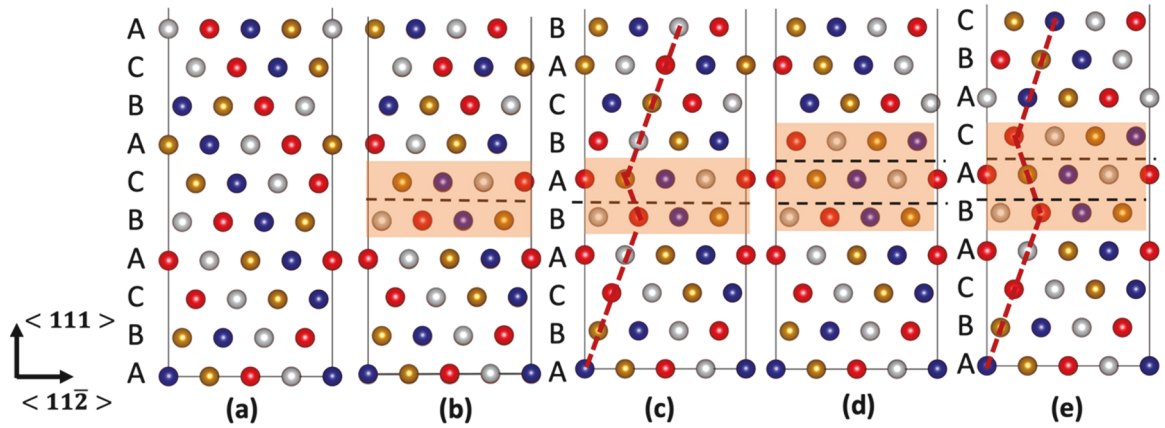

Fig. 2. Atomic structures of simulation slabs consisting of sequentially packed {111} atomic layers to model (a) perfect fcc crystal structure, (b) unstable stacking fault, (c) intrinsic stacking fault, (d) unstable twinning, and (e) extrinsic stacking fault in CoCrFeNi HEA. In this figure, the blue, red, brown, and grey balls represent Co, Cr, Fe, and Ni atoms, respectively.

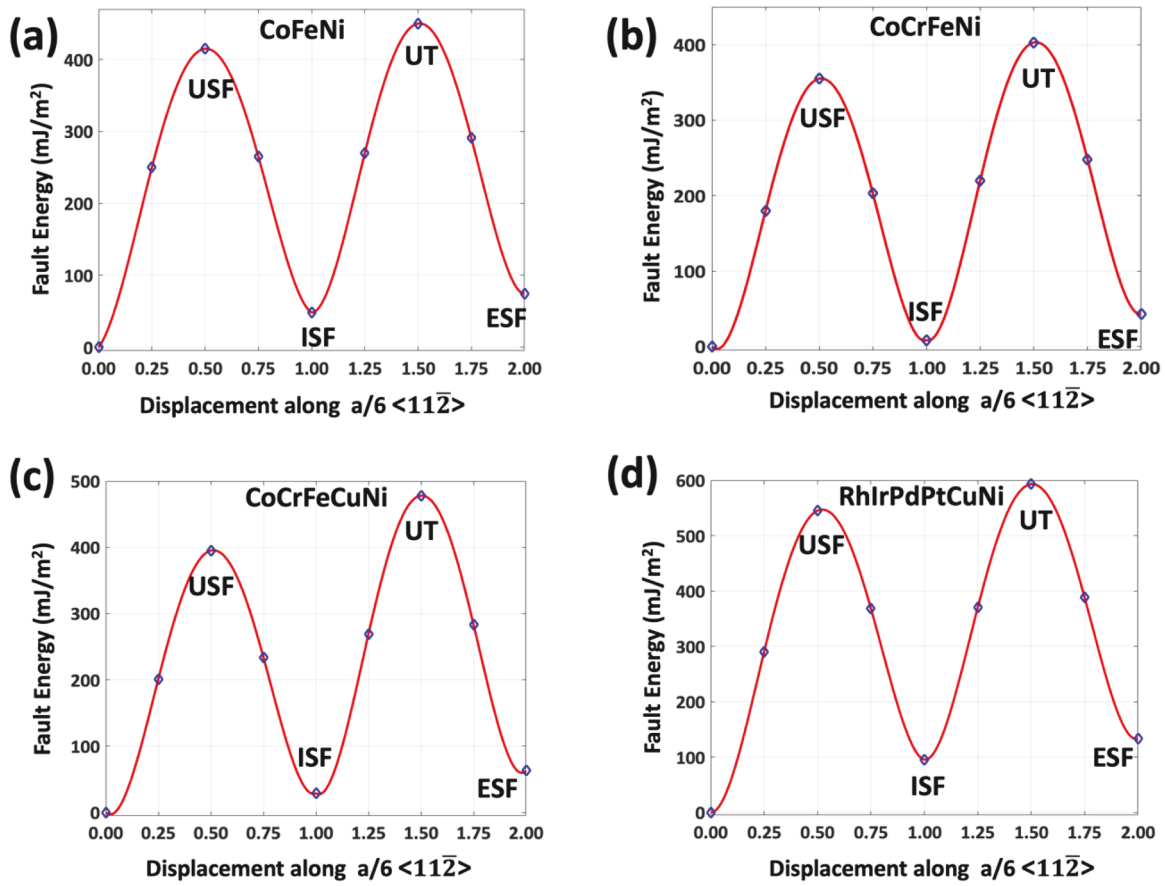

Fig. 3. Predicted generalized stacking fault energy curve (from O to ISF) and generalized planar fault energy curve (from ISF to ESF) of (a) CoFeNi, (b)CoCrFeNi, (c) CoCrFeCuNi, and (d) RhIrPdPtCuNi alloys.

we predict for CoFeNi alloy the ISF energy to be 48 mJ/m^2, which is comparable to previous result of 65 mJ/m^2 [41]. We predict for CoCrFeCuNi alloy the ISF energy to be 32 mJ/m^2 close to the reported value of 27.5 mJ/m^2 [34]. We predict for RhIrPdPtNiCu alloy the ISF energy to be 95 mJ/m^2 as compared to a previous result of 138 mJ/m^2 [18]. There have been many previous studies on the stacking fault energies of CoCrFeNi alloy. The literature values vary from − 180–34.3 mJ/m^2 for ISF energy [27,28,41–43]. In this study we predict for CoCrFeNi alloy the ISF energy to be 10 mJ/m^2, which is within the range of the literature values.

The plastic deformation of fcc metals is primarily through deformation twinning and dislocation motion. Tadmor and Bernstein [44] proposed to employ a parameter called twinnability (τ_α) to describe the tendency of deformation twinning relative to dislocation-mediated slip during the plastic deformation of fcc metals. Twinnability is a material property related to the stacking fault energies and can be approximated by the following analytical expression.

$$\tau_\alpha = [1.136 - 0.151\frac{\gamma_{isf}}{\gamma_{usf}}]\sqrt{\frac{\gamma_{usf}}{\gamma_{ut}}} \quad (1)$$

where γ_{isf}, γ_{usf}, and γ_{ut} refer to the energy of ISF, USF, and UT, respectively.

In this study, we predict the values of twinnability to be 1.082 for CoFeNi, 1.056 CoCrFeNi, 1.045 for RhIrPdPtNiCu, and 0.982 for CoCrFeCuNi. In Ref. [44], the twinnability was predicted to be 1.044 for pure Ag and 0.965 for Au. Therefore, the deformation twinning is predicted to be easier in CoFeNi, CoCrFeNi, and RhIrPdPtNiCu alloys similar to that in metal Ag, whereas dislocation motion is favored in CoCrFeCuNi alloy similar to that in metal Au. It is worth mentioning that deformation twinning has been clearly observed during the plastic deformation of metal Ag [45,46] whereas extensive dislocation slip was observed during the plastic deformation of metal Au. [47] Our predictions in this study appear to agree well with a previous report that deformation twinning was observed in CoCrFeNi alloys under strain using high-resolution TEM [48].

3.3. Yield strength predictions

In fcc metals, a full dislocation with a Burger vector of a/2 < 110 > would dissociate into two Shockley partials separated by a segment of stacking fault within the (111) slip plane. [49] The displacement induced by such a pair of partial dislocations in a crystal could be written as [50]:

$$u_x(x) = \frac{b}{2\pi}(arctan\frac{x-\frac{d_x}{2}}{w_x} + arctan\frac{x+\frac{d_x}{2}}{w_x}) + \frac{b}{2} \quad (2)$$

where x represents the distance to the middle point of the two partial dislocations along the Burgers vector direction [1$\bar{1}$0] within a (111) plane, b is the length of the Burgers vector, d_x is the separation between the two partial dislocations, w_x is the half width of the partial dislocations. The value of d_x and w_x can be estimated by $d_x/b = 1.618(\gamma_{usf}/\gamma_{isf}) + 2.1335$ and $w_x/b = \frac{-546\gamma_{isf}}{C_{44}b} + 11$. [51,52].

Peierls stress (τ_p) is the critical resolved shear stress required to resist dislocation motion and has been proposed to be determined from GSFE curves (also called γ surface) [50]. In the framework of the Peierls model based on general dislocations with both screw and edge components, the GSFE surface for {111} plane in a cubic crystal could be expanded in 2D Fourier series [53]:

$$\begin{aligned}\gamma(u_x,u_z) = C_0 &+ C_1[\cos(2qu_z)+\cos(pu_x+qu_z)+\cos(-pu_x+qu_z)]\\ &+ C_2[\cos(2pu_x)+\cos(pu_x+3qu_z)+\cos(-pu_x+3qu_z)]\\ &+ C_3[\cos(4qu_z)+\cos(2pu_x+2qu_z)+\cos(pu_x-2qu_z)]\\ &+C_4[\cos(3pu_x+qu_z)+\cos(3pu_x-qu_z)+\cos(2pu_x+4qu_z)\\ &+\cos(2pu_x-4qu_z)+\cos(pu_x+5qu_z)+\cos(-pu_x+5qu_z)]\end{aligned} \quad (3)$$

where $p = 2\pi/b$, $q=2\pi/\sqrt{3}b$. Specifically, for fcc metals, the screw components of the dislocations are negligible. Hence, we set u_z as zero and only considered the displacement u_x in Eq. (3).

In the Perierls-Nabarrro model [54], the misfit energy is calculated as the sum of the lattice misfit energy between atomic planes,

$$W(\mu) = \sum_{m=-\infty}^{\infty}\gamma(f(m\Delta d-\mu))\Delta d \quad (4)$$

where μ represents the shift of dislocation center, and Δd is the spacing of adjacent atomic planes in the $[11\bar{2}]$ direction in a perfect fcc crystal ($\sqrt{6}a/4$ with a as the lattice parameter of the fcc crystal). Thus, the Peierls stress is the maximum of resistant stress required to overcome the barrier in $W(\mu)$,

$$\tau_p = \max\{\frac{1}{b}\frac{dW}{d\mu}\} \quad (5)$$

Following the computational method proposed by Kamimura et al. [55], we numerically fitted $W(\mu)$ using Fourier series to the third order and determined the values of the Peierls stress converged with respect to increasing value of m.

Furthermore, we extended this computational approach to predict the critical twinning stress (τ_{tw}) from our predicted GPFE curve which is also considered as a γ surface. For the twinning stress prediction, we adjusted the expression of d_x and w_x as $d_x/b = 1.618[(\gamma_{ut}-\gamma_{isf})/(\gamma_{esf}-\gamma_{isf})]+2.1335$ and $w_x/b=\frac{-546(\gamma_{esf}-\gamma_{isf})}{C_{44}b}+11$. Thus, the critical twinning stress (τ_{tw}) can be calculated in the same manner showed in Eqs. (4) and (5).

In this study, we calculated the values of τ_p from the GSFE curves which are the parts from a perfect crystal (i.e., origin O) to ISF in Fig. 3 and the values of τ_{tw} from the GPFE curves which are the parts from ISF to ESF in Fig. 3 for CoFeNi, CoCrFeNi, CoCrFeCuNi, and RhIrPdPtNiCu alloys. Our predictions are presented in Table 2.

Our results in Table 2 indicate that τ_p is predicted to have a higher value than τ_{tw} for CoFeNi, CoCrFeNi, and RhIrPdPtNiCu alloys. These computational predictions suggest that the deformation twinning (i.e., ESF) should be easy to form after a single layer stacking fault (i.e., ISF) is formed by overcoming τ_p in these three HEAs. In contrast, we predict in Table 2 that it requires an even higher shearing stress (202 MPa) to form a two-layer deformation twin after overcoming τ_p (195 MPa) to form a single-layer stacking fault in CoCrFeCuNi alloy. Consequently, it can be inferred from the computational results in Table 2 that deformation twinning could be the primary plastic deformation mode in CoFeNi, CoCrFeNi, and RhIrPdPtNiCu alloys whereas dislocation slipping be the primary plastic deformation mode in CoCrFeCuNi alloy. This finding agrees well with the predictions based on the parameter twinnability proposed by Tadmor and Bernstein [44].

Furthermore, we used the calculated Peierls stress (τ_p) of the single crystal HEAs in Table 2 to estimate the yield strengths of the four HEAs in their polycrystal forms. In this work, we consider two main contributions (i.e., intrinsic strength and grain size effect) to the yield strength of the alloys. The intrinsic strength of polycrystal fcc metals is proposed to be related to the Peierls stress in single crystal in an empirical relation as shown [56].

Table 2
Predicted Peierls stress (τ_p) and critical twinning stress (τ_{tw}) (in unit of MPa) of four fcc HEAs.

	CoFeNi	CoCrFeNi	CoCrFeCuNi	RhIrPdPtNiCu
τ_p	210	240	195	484
τ_{tw}	201	232	202	459

Table 3
Predicted intrinsic strength, grain size effect, and yield strength (in unit of MPa) of four HEAs. The experimental and computational values of yield strength from the literature are included for comparison.

	CoFeNi	CoCrFeNi	CoCrFeCuNi	RhIrPdPtNiCu
Intrinsic strength	214	245	199	494
Grain size effect	18	23	13	26
Yield Strength	232	268	212	520
Experiment	211[62]	275[32]	230[62]	527[18]
Computation		201[63]		583[18]

$$\sigma_{y0} = \frac{1}{3}M\tau_p \quad (6)$$

where M= 3.06 is the Taylor factor of fcc polycrystals [57].

The grain size effect to the yield strength is because that the grain boundaries in polycrystal samples will present obstacles to the motion of dislocations and/or deformation twins and can be described by a theoretical model as presented in Ref. [58]. Hence, we can estimate the yield strength of a polycrystal fcc metal using the following equation.

$$\sigma_y = \sigma_{y0} + M\sqrt{\frac{Gb\tau_p}{2\pi d}} \quad (7)$$

Since Gb here represents the energy of a dislocation in an fcc metal, the value of G is taken as the value of C_{44} of single crystal. Typical grain size of HEAs is in the order of 1–100 μm [59–61], consequently we chose a median value of grain size d= 50 μm in this study.

In Table 3, we present our predicted yield strengths of CoFeNi, CoCrFeNi, CoCrFeCuNi, and RhIrPdPtNiCu alloys. In comparison to the corresponding experimentally measured values, our predicted yield strength of RhIrPdPtNiCu alloy differs by 1.3% (the best case among the four HEAs) and the yield strength of CoFeNi alloy differs by 10.0% (the worst case among the four HEAs). It appears that our predictions are in quite good agreement with experimental values [18,32,62]. In comparison to the available computational predictions based on solid solution strengthening theory, our predicted yield strength of RhIrPdPtNiCu alloy differs by 10.8% and the yield strength of CoCrFeNi alloy differs by 33.3%. It should be noted that our computational method is based on rigid slip of two half-crystals as manifested in the generalized stacking fault energy and generalized planar fault energy curves, whereas the previous computational method [18,63] was derived based on solute strengthening theory of dislocations in fcc metals.

4. Conclusion

In summary, we have developed the first principles based computational methods to predict the mechanical properties, including elastic constants, Young's and shear modulus, stacking fault energies, twinnability parameter, Peierls stress and critical twinning stress, and yield strength, of the HEAs with fcc crystal structure. In order to demonstrate the reliability of these computational methods, we applied the computational methods to four different types of fcc HEAs, namely, ternary CoFeNi, quaternary CoCrFeNi, quinary CoCrFeCuNi, and senary RhIrPdPtNiCu alloys. Our predicted mechanical properties of the four HEAs are found to be in good agreement with available experimental values.

Specifically for fcc metals, we validated a computational approach to derive the Peierls stress of edge dislocations from the calculated generalized stacking fault energy curves and the critical stress for deformation twinning formation from the calculated generalized planar fault energy curves on (111) planes. Moreover, comparison of the predicted values of Peierls stress and critical twinning stress reveals that deformation twinning could be the primary plastic deformation mode in

CoFeNi, CoCrFeNi, and RhIrPdPtNiCu alloys whereas dislocation slipping be the primary plastic deformation mode in CoCrFeCuNi alloy. This prediction is in consistent with some available experimental observation and the predictions from the Tadmor-Bernstein twinnability parameters. Therefore, our computational approach could not only provide accurate values for the mechanical properties but also provide insights to the plastic deformation mechanisms of fcc HEAs.

HEAs have been found to have exceptional mechanical properties which are also tunable by their chemical composition. This work develops a rigorous computational framework, validates the computation methods by four fcc HEAs, and thus paves the road for future studies to correlate the chemical composition and mechanical properties of fcc HEAs. Consequently, this study provides reliable computational tools for rational design of HEAs based on the first principles calculations.

CRediT authorship contribution statement

Siming Zhang: Investigation, Method development, Data curation, Writing – original draft. **Guofeng Wang:** Conceptualization, Supervision, Writing – review & editing.

Declaration of Competing Interest

The authors declare that they have no known competing financial interests or personal relationships that could have appeared to influence the work reported in this paper.

Data Availability

Data will be made available on request.

Acknowledgements

Financial support for this research provided by the National Science Foundation (NSF) (grant number DMR 1905572) is gratefully acknowledged. This work also used the computational resources provided by the University of Pittsburgh Center for Research Computing and the Extreme Science and Engineering Discovery Environment (XSEDE) supported by National Science Foundation grant number ACI-1053575.

References

[1] J.-W. Yeh, S.-K. Chen, S.-J. Lin, J.-Y. Gan, T.-S. Chin, T.-T. Shun, C.-H. Tsau, S.-Y. Chang, Nanostructured high-entropy alloys with multiple principal elements: novel alloy design concepts and outcomes, Adv. Eng. Mater. 6 (5) (2004) 299–303, https://doi.org/10.1002/adem.200300567.

[2] E.P. George, W.A. Curtin, C.C. Tasan, High entropy alloys: a focused review of mechanical properties and deformation mechanisms, Acta Mater. 188 (2020) 435–474, https://doi.org/10.1016/j.actamat.2019.12.015.

[3] E.P. George, D. Raabe, R.O. Ritchie, High-entropy alloys, Nat. Rev. Mater. 4 (2019) 515–534, https://doi.org/10.1038/s41578-019-0121-4.

[4] B. Gludovatz, A. Hohenwarter, K.V.S. Thurston, H. Bei, Z. Wu, E.P. George, R. O. Ritchie, Exceptional damage-tolerance of a medium-entropy alloy CrCoNi at cryogenic temperatures, Nat. Commun. 7 (2016) 10602, https://doi.org/10.1038/ncomms10602.

[5] F. Otto, Y. Yang, H. Bei, E.P. George, Relative effects of enthalpy and entropy on the phase stability of equiatomic high-entropy alloys, Acta Mater. 61 (7) (2013) 2628–2638, https://doi.org/10.1016/j.actamat.2013.01.042.

[6] W. Li, P.K. Liaw, Y. Gao, Fracture resistance of high entropy alloys: a review, Intermetallics 99 (2018) 69–83, https://doi.org/10.1016/j.intermet.2018.05.013.

[7] BS EN 10088–4:2009 Stainless steels. Technical delivery conditions for sheet/plate and strip of corrosion resisting steels for construction purposes, BSI.

[8] M.P. Agustianingrum, I. Ondicho, D.E. Jodi, N. Park, U. Lee, Theoretical evaluation of solid solution interaction in $Fe_x(CoCrMnNi)_{100-x}$ medium- and high-entropy alloys, Mater. Sci. Eng. A 759 (2019) 633–639, https://doi.org/10.1016/j.msea.2019.05.082.

[9] M.P. Agustianingrum, S. Yoshida, N. Tsuji, N. Park, Effect of aluminum addition on solid solution strengthening in CoCrNi medium-entropy alloy, J. Alloy. Compd. 781 (2019) 866–872, https://doi.org/10.1016/j.jallcom.2018.12.065.

[10] H. Zhang, X. Sun, Song Lu, Z. Dong, X. Ding, Y. Wang, L. Vitos, Elastic properties of $Al_xCrMnFeCoNi$ ($0 < x < 5$)) high-entropy alloys from ab initio theory, Acta Mater. 155 (2018) 12–22, https://doi.org/10.1016/j.actamat.2018.05.050.

[11] K. Tanaka, T. Teramoto, R. Ito, Monocrystalline elastic constants of fcc CrMnFeCoNi high entropy alloy, MRS Adv. 2 (27) (2017) 1429–1434, https://doi.org/10.1557/adv.2017.76.

[12] A. Haglund, M. Koehler, D. Catoor, E.P. George, V. Keppens, Polycrystalline elastic moduli of a high-entropy alloy at cryogenic temperatures, Intermetallics 58 (2015) 62–64, https://doi.org/10.1016/j.intermet.2014.11.005.

[13] F. Tian, L.K. Varga, J. Shen, L. Vitos, Calculating elastic constants in high-entropy alloys using the coherent potential approximation: Current issues and errors, Comput. Mater. Sci. 111 (2016) 350–358, https://doi.org/10.1016/j.commatsci.2015.09.058.

[14] Z. Wu, H. Bei, G.M. Pharr, E.P. George, Temperature dependence of the mechanical properties of equiatomic solid solution alloys with face-centered cubic crystal structures, Acta Mater. 81 (2014) 428–441, https://doi.org/10.1016/j.actamat.2014.08.026.

[15] A. Zunger, S.-H. Wei, L.G. Ferreira, JamesE. Bernard, Special quasirandom structures, Phys. Rev. Lett. 65 (1990) 353–356, https://doi.org/10.1103/PhysRevLett.65.353.

[16] S.-H. Wei, L.G. Ferreira, E. James, Bernard, Alex Zunger, Electronic properties of random alloys: special quasirandom structures, Phys. Rev. B 42 (9622) (1990) 9622–9649, https://doi.org/10.1103/PhysRevB.42.9622.

[17] G. Kim, H. Diao, C. Lee, A.T. Samaei, T. Phana, M. de Jong, K. An, D. Ma, P.K. Liaw, W. Chen, First-principles and machine learning predictions of elasticity in severely lattice-distorted high-entropy alloys with experimental validation, Acta Mater. 181 (2019) 124–138, https://doi.org/10.1016/j.actamat.2019.09.026.

[18] B. Yin, W.A. Curtin, First-principles-based prediction of yield strength in the RhIrPdPtNiCu high-entropy alloy, npj Comput. Mater. 5 (2019) 14, https://doi.org/10.1038/s41524-019-0151-x.

[19] B. Yin, Shuhei Yoshida, Nobuhiro Tsuji, W.A. Curtin, Yield strength and misfit volumes of NiCoCr and implications for short-range-order, Nat. Commun. 11 (2020) 2507, https://doi.org/10.1038/s41467-020-16083-1.

[20] G. Kresse, J. Furthmüller, Efficient iterative schemes for ab initio total energy calculations using a plane-wave basis set, Phys. Rev. B 54 (1996) 11169–11186, https://doi.org/10.1103/PhysRevB.54.11169.

[21] G. Kresse, D. Joubert, From ultra-soft pseudopotentials to the projector augmented-wave method, Phys. Rev. B 59 (1999) 1758–1775, https://doi.org/10.1103/PhysRevB.59.1758.

[22] J.P. Perdew, K. Burke, M. Ernzerhof, Generalized gradient approximation made simple, Phys. Rev. Lett. 77 (1996) 3865–3868, https://doi.org/10.1103/PhysRevLett.77.3865.

[23] H.J. Monkhorst, J.D. Pack, Special points for Brillouin-zone integrations, Phys. Rev. B 13 (1976) 5188–5192, https://doi.org/10.1103/PhysRevB.13.5188.

[24] A. van de Walle, P. Tiwary, M. de Jong, D.L. Olmsted, M. Asta, A. Dick, D. Shin, Y. Wang, L.-Q. Chen, Z.-K. Liu, Efficient stochastic generation of special quasi-random structures, Calphad 42 (2013) 13–18, https://doi.org/10.1016/j.calphad.2013.06.006.

[25] H. Song, F. Tian, Q.-M. Hu, L. Vitos, Y. Wang, J. Shen, N. Chen, Local lattice distortion in high-entropy alloys, Phys. Rev. Mater. 1 (2017), 023404, https://doi.org/10.1103/PhysRevMaterials.1.023404.

[26] T.T. Zuo, R.B. Li, X.J. Ren, Y. Zhang, Effects of Al and Si addition on the structure and properties of CoFeNi equal atomic ratio alloy, J. Magn. Magn. Mater. 371 (2014) 60–68, https://doi.org/10.1016/j.jmmm.2014.07.023.

[27] M. Beyramali Kivy, M.Asle Zaeem, Generalized stacking fault energies, ductilities, and twinnabilities of CoCrFeNi-based face-centered cubic high entropy alloys, Scr. Mater. 139 (2017) 83–86, https://doi.org/10.1016/j.scriptamat.2017.06.014.

[28] Y.H. Zhang, Y. Zhuang, A. Hu, J.J. Kai, C.T. Liu, The origin of negative stacking fault energies and nano-twin formation in face-centered cubic high entropy alloys, Scr. Mater. 130 (2017) 96–99, https://doi.org/10.1016/j.scriptamat.2016.11.014.

[29] F. He, Z. Wang, Q. Wu, J. Li, J. Wang, C.T. Liu, Phase separation of metastable CoCrFeNi high entropy alloy at intermediate temperatures, Scr. Mater. 126 (2017) 15–19, https://doi.org/10.1016/j.scriptamat.2016.08.008.

[30] X.F. Wang, Y. Zhang, Y. Qiao, G.L. Chen, Novel microstructure and properties of multicomponent $CoCrCuFeNiTi_x$ alloys, Intermetallics 15 (2007) 357–362, https://doi.org/10.1016/j.intermet.2006.08.005.

[31] P. Söderlind, O. Eriksson, J.M. Wills, A.M. Boring, Theory of elastic constants of cubic transition metals and alloys, Phys. Rev. B 48 (1993) 5844–5851, https://doi.org/10.1103/PhysRevB.48.5844.

[32] C. Niu, A.J. Zaddach, C.C. Koch, D.L. Irving, First principles exploration of near-equiatomic NiFeCrCo high entropy alloys, J. Alloy. Compd. 672 (2016) 510–520, https://doi.org/10.1016/j.jallcom.2016.02.108.

[33] S. Huang, A. Vida, A. Heczel, E. Holmstrom, L. Vitos, Thermal expansion, elastic and magnetic properties of FeCoNiCu-based high-entropy alloys using first-principle theory, JOM 69 (2017) 2107–2112, https://doi.org/10.1007/s11837-017-2565-6.

[34] M. Jamal, S.Jalali Asadabadi, Iftikhar Ahmad, H.A. Rahnamaye Aliabad, Elastic constants of cubic crystals, Comput. Mater. Sci. 95 (2014) 592–599, https://doi.org/10.1016/j.commatsci.2014.08.027.

[35] G. Laplanche, P. Gadaud, C. Bärsch, K. Demtröder, C. Reinhart, J. Schreuer, E. P. George, Elastic moduli and thermal expansion coefficients of medium-entropy subsystems of the CrMnFeCoNi high-entropy alloy, J. Alloy. Compd. 746 (2018) 244–255, https://doi.org/10.1016/j.jallcom.2018.02.251.

[36] T. Górecki, The relations between the shear modulus, the bulk modulus and young's modulus for polycrystalline metallic elements, Mater. Sci. Eng. 43 (1980) 225–230, https://doi.org/10.1016/0025-5416(80)90106-8.

[37] Springer Handbook of Materials Data, ISBN: 978–3-319–69741-3, © Springer Nature Switzerland AG 2018.

[38] C.J. Smithells, Metals reference book, 7th edition, 1992 ISBN 0 7506 3624 6.

[39] M. Jafary-Zadeh, K.H. Khoo, R. Laskowski, P.S. Branicio, A.V. Shapeev, Applying a machine learning interatomic potential to unravel the effects of local lattice distortion on the elastic properties of multi-principal element alloys, J. Alloy. Compd. 803 (2019) 1054–1062, https://doi.org/10.1016/j.jallcom.2019.06.318.
[40] Qin Yu Jun Ding, Mark Asta, Robert O. Ritchie, Tunable stacking fault energies by tailoring local chemical order in CrCoNi medium-entropy alloys, PNAS 115 (36) (2018) 8919–8924, https://doi.org/10.1073/pnas.1808660115.
[41] S. Zhao, G. Malcolm Stock, Y. Zhang, Stacking fault energies of face-centered cubic concentrated solid solution alloys, Acta Mater. 134 (2017) 334–345, https://doi.org/10.1016/j.actamat.2017.05.001.
[42] A.J. Zaddach, C. Niu, C.C. Koch, D.L. Irving, Mechanical properties and stacking fault energies of NiFeCrCoMn high-entropy alloy, JOM 65 (12) (2013) 1780–1789, https://doi.org/10.1007/s11837-013-0771-4.
[43] H. Huang, X. Li, Z. Dong, W. Li, S. Huang, D. Meng, X. Lai, T. Liu, S. Zhu, L. Vitos, Critical stress for twinning nucleation in CrCoNi-based medium and high entropy alloys, Acta Mater. 149 (2018) 388–396, https://doi.org/10.1016/j.actamat.2018.02.037.
[44] E.B. Tadmor, N. Bernstein, A First-principles measure for the twinnability of FCC metals, J. Mech. Phys. Solids 52 (2004) 2507–2519, https://doi.org/10.1016/j.jmps.2004.05.002.
[45] X. Huang, W. Yang, R. Harder, Y. Sun, M. Lu, Y.S. Chu, I.K. Robinson, H. Mao, Deformation twinning of a silver nanocrystal under high pressure, Nano Lett. 15 (11) (2015) 7644–7649, https://doi.org/10.1021/acs.nanolett.5b03568.
[46] J. Gubicza, N.Q. Chinh, J.L. Labar, Z. Hegedus, T.G. Langdon, Twinning and dislocation activity in silver processed by severe plastic deformation, J. Mater. Sci. 44 (2009) 1656–1660, https://doi.org/10.1007/s10853-009-3278-1.
[47] R. Dou, B. Derby, The strength of gold nanowire forests, Scr. Mater. 59 (2) (2008) 151–154, https://doi.org/10.1016/j.scriptamat.2008.02.046.
[48] W. Wu, M. Song, S. Ni, J. Wang, Y. Liu, B. Liu, X. Liao, Dual mechanisms of grain refinement in a FeCoCrNi high entropy alloy processed by high pressure torsion, Sci. Rep. 7 (2017) 46720, https://doi.org/10.1038/srep46720.
[49] J.P. Hirth, J. Lothe, Theory of Dislocations, McGraw-Hill, New York, 1967.
[50] S.H. Zhang, I.J. Beyerlein, D. Legut, Z.H. Fu, Z. Zhang, S.L. Shang, Z.K. Liu, T. C. Germann, R.F. Zhang, First-principles investigation of strain effects on the stacking fault energies, dislocation core structure, and Peierls stress of magnesium and its alloys, Phys. Rev. B 95 (2017), 224106, https://doi.org/10.1103/PhysRevB.95.224106.
[51] A. Hunter, R.F. Zhang, I.J. Beyerlein, Dependence of equilibrium stacking fault width in fcc metals on the γ-surface, Model. Simul. Mater. Sci. Eng. 21 (2013), 025015 https://10.1088/0965-0393/21/2/025015.
[52] A. Hunter, R.F. Zhang, I.J. Beyerlein, The core structure of dislocations and their relationship to the material γ-surface, J. Appl. Phys. 115 (2014), 134314, https://doi.org/10.1063/1.4870462.
[53] G. Schoeck, The core structure, recombination energy and Peierls energy for dislocations in Al, Philos. Mag. A 81 (2001) 1161–1176, https://doi.org/10.1080/01418610108214434.
[54] B. Joos, M.S. Duesbery, The peierls stress of dislocations: an analytic formula, Phys. Rev. Lett. 78 (1997) 266–269, https://doi.org/10.1103/PhysRevLett.78.266.
[55] Y. Kamimura, K. Edagawa, A.M. Iskandarov, M. Osawa, Y. Umeno, S. Takeuchi, Peierls stresses estimated via the Peierls-Nabarro model using ab-initio γ-surface and their comparison with experiments, Acta Mater. 148 (2018) 355–362, https://doi.org/10.1016/j.actamat.2018.02.009.
[56] K.W. Siu, A. Ngan, Relation between yield stress and peierls stress, Phys. Status Solidi B 256 (2019) 1900107, https://doi.org/10.1002/pssb.201900107.
[57] T.H. Courtney. Mechanical Behavior of Materials, second ed., McGraw Hill Education, New York, 2012.
[58] T.T. Zhu, A.J. Bushby, D.J. Dunstan, Materials mechanical size effects: a review, Mater. Technol. 23 (4) (2008) 193–209, https://doi.org/10.1179/175355508×376843.
[59] Z. Wu, H. Bei, F. Otto, G.M. Pharr, E.P. George, Recovery, recrystallization, grain growth and phase stability of a family of FCC-structured multi-component equiatomic solid solution alloys, Intermetallics 46 (2014) 131–140, https://doi.org/10.1016/j.intermet.2013.10.024.
[60] X. Qin, Yi Xu, Y. Sun, H. Fujii, Z. Zhu, C.H. Shek, Effect of process parameters on microstructure and mechanical properties of friction stir welded CoCrFeNi high entropy alloy, Mater. Sci. Eng. A 782 (2020), 139277, https://doi.org/10.1016/j.msea.2020.139277.
[61] X. Yan, X. Zhang, F. Wang, T. Stockdale, Y. Dzenis, M. Nastasi, B. Cui, Fabrication of ODS austenitic steels and CoCrFeNi high-entropy alloys by spark plasma sintering for nuclear energy applications, JOM 71 (2019) 2856–2867, https://doi.org/10.1007/s11837-019-03531-7.
[62] S. Gorsse, M.H. Nguyen, O.N. Senkov, D.B. Miracle, Database on the mechanical properties of high entropy alloys and complex concentrated alloys, Data Brief. 21 (2018) 2664–2678, https://doi.org/10.1016/j.dib.2018.11.111.
[63] B. Yin, W.A. Curtin, Origin of high strength in the CoCrFeNiPd high-entropy alloy, Mater. Res. Lett. 8 (6) (2020) 209–215, https://doi.org/10.1080/21663831.2020.1739156.